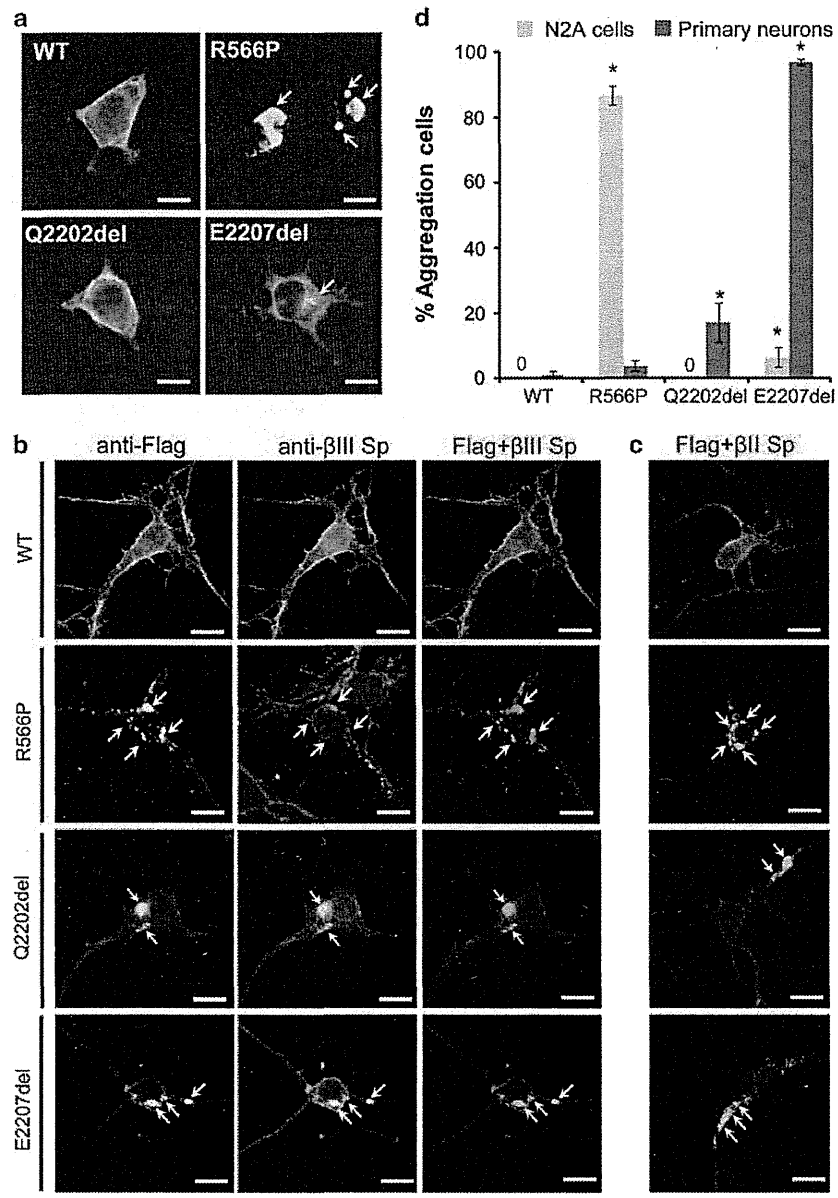

Figure 3 Mutant α-II spectrin cause aggregation of α/β spectrin heterodimers. **(a)** The wildtype (WT) and the three mutant α-II spectrins were detected by immunofluorescence in transfected N2A cells. The WT α-II spectrin and p.Q2202del mutant were similarly expressed at cell periphery. However, the p.R566P and p.E2207del α-II spectrin mutants showed large and small aggregations (arrows), respectively. **(b, c)** Expression of the WT and the three mutant α-II spectrins at 7 days *in vitro* in primary cortical neurons. Flag tagged WT α-II spectrin was expressed at cell extensions and periphery, overlapping with the expression of β-II and β-III spectrins. Three mutant α-II spectrins (R566P, Q2202del, and E2207del) showed aggregation in cell bodies and neurites (arrows). Aggregations caused by the Q2202del and E2207del mutants were colocalized with both β-II and β-III spectrins (lower two panels). Aggregations caused by the R566P mutant were colocalized with β-II spectrin, but their colocalization with β-III spectrin was not evident. The scale bar represents 10 μm. **(d)** N2A cells and primary cortical neurons showing α-II spectrin aggregation were counted: Numbers of aggregated/total numbers of counted cells (expressing transfected α-II spectrin) in three experiments: N2A, WT: 0/194, R566P: 212/244, Q2202del: 0/241, E2207del: 9/180; primary neurons, WT: 3/300, R566P: 11/300, Q2202del: 51/300, E2207del: 291/300. Asterisks indicate that a significant difference ($P<0.01$) was observed compared with WT by Bonferroni's posttest analysis. The scale bar represents 10 μm.

that of p.E2207del, it was observed at a lower frequency correlating with the less severe phenotype observed in patient-2. Heterozygous mutations in β-III spectrin (*SPTBN2*) were previously shown to cause spinocerebellar ataxia type-5.[3] It is tempting to speculate that cerebellar atrophy in patients with mutations in *SPTAN1* is caused at least in part by the aggregation of β-III spectrin. This is consistent with the fact that β-III, unlike β-II spectrin, is abundantly expressed in the human cerebellum (Allen Brain Atlas; http://human.brain-map.org/). All together, these observations strengthen the causal relationship between in-frame mutations at the C-terminus of SPTAN1, severe ID, and pontocerebellar atrophy, while expanding the phenotypical spectrum associated with these mutations.

We also identified a *de novo* missense (p.R566P) in *SPTAN1* in a patient with mild non-syndromic ID without epilepsy or any gross brain abnormalities. Interestingly, the aggregation profiles induced by p.R566P and by the in-frame mutations are different. First, p.R566P induced aggregates in a great proportion of N2A cells but only in a negligible proportion of primary neuronal cells. The reverse pattern was found with the in-frame mutations. Second, p.R566P only aggregated with β-II spectrin whereas the in-frame mutations showed aggregations with both β-II and β-III spectrin subunits in cortical neurons. The phenotypic differences between the patient with the missense and the patients with the in-frame mutations may thus be explained by the preferential aggregation of p.R566P α-II with β-II spectrin. It is important to underline that the sister of patient-1 was also diagnosed with non-syndromic ID but lacked p.R566P in her blood DNA. Although it is possible that she is a phenocopy, it appears more likely that p.R566P is not responsible for her brother's condition. The identification of other patients with deleterious mutations in the N-terminal region of SPTAN1 would help to distinguish these possibilities.

In summary, our work indicates that in-frame mutations in the C-terminus of SPTAN1 cause a core set of manifestations that include severe ID, generalized epilepsy, and pontocerebellar atrophy. Although it is unclear whether p.R566P is pathogenic, we found that this mutation induces a distinct pattern of spectrin aggregation. Additional studies are needed to determine whether this pattern of aggregation is associated with a specific phenotype. Our study thus provides a paradigm to validate candidate variants in *SPTAN1* and to establish correlations between genotypes and phenotypes.

CONFLICT OF INTEREST

The authors declare no conflict of interest

ACKNOWLEDGEMENTS

This study is supported by grants from the Canadian Institute of Health Research (CIHR) (J Michaud, G Rouleau, J-C Lacaille), Réseau de Génétique Médicale Appliquée (RMGA)/Fonds de la Recherche en Santé du Québec (FRSQ) (J Michaud), Genome Canada and Genome Quebec and co-funding by Université de Montréal for the Synapse to diseases (S2D) project (G Rouleau), the Ministry of Health, Labour and Welfare (H Saitsu, N Matsumoto), the Japan Science and Technology Agency (N Matsumoto), a Grant-in-Aid for Scientific Research from the Japan Society for the Promotion of Science (N Matsumoto), and a Grant-in-Aid for Young Scientist from the Japan Society for the Promotion of Science (H Saitsu). J Michaud is the recipient of a Clinical Investigatorship Award of the CIHR (Institute of Genetics) and of a Senior Scientist Award from FRSQ. G Rouleau holds the Canada Research Chair and a Jeanne-et-J-Louis-Levesque Chair for the Genetics of Brain Diseases. We are grateful for the dedicated work of members of the S2D team (CHUM Notre-Dame Hospital Research Center, Montreal), including management (Claude Marineau and Ronald Lafrenière) and bioinformatics (Edouard Henrion and Ousmane Diallo). We are thankful for the efforts of the members of McGill University and Génome Québec Innovation Centre Sequencing and Bioinformatics groups.

1 Bennett V, Healy J: Organizing the fluid membrane bilayer: diseases linked to spectrin and ankyrin. *Trends Mol Med* 2008; **14**: 28–36.
2 Baines AJ: Evolution of spectrin function in cytoskeletal and membrane networks. *Biochem Soc Trans* 2009; **37**: 796–803.
3 Ikeda Y, Dick KA, Weatherspoon MR *et al*: Spectrin mutations cause spinocerebellar ataxia type 5. *Nat Genet* 2006; **38**: 184–190.
4 Saitsu H, Tohyama J, Kumada T *et al*: Dominant-negative mutations in alpha-II spectrin cause West syndrome with severe cerebral hypomyelination, spastic quadriplegia, and developmental delay. *Am J Hum Genet* 2010; **86**: 881–891.
5 Speicher DW, Weglarz L, DeSilva TM: Properties of human red cell spectrin heterodimer (side-to-side) assembly and identification of an essential nucleation site. *J Biol Chem* 1992; **267**: 14775–14782.
6 Conrad DF, Keebler JE, DePristo MA *et al*: Variation in genome-wide mutation rates within and between human families. *Nat Genet* 2011; **43**: 712–714.
7 Hamdan FF, Gauthier J, Araki Y *et al*: Excess of *de novo* deleterious mutations in genes associated with glutamatergic systems in nonsyndromic intellectual disability. *Am J Hum Genet* 2011; **88**: 306–316.
8 Vissers LE, de Ligt J, Gilissen C *et al*: A *de novo* paradigm for mental retardation. *Nat Genet* 2010; **42**: 1109–11012.
9 Saitsu H, Kato M, Mizuguchi T *et al*: *De novo* mutations in the gene encoding STXBP1 (MUNC18-1) cause early infantile epileptic encephalopathy. *Nat Genet* 2008; **40**: 782–788.
10 Ng PC, Henikoff S: SIFT: predicting amino acid changes that affect protein function. *Nucleic Acids Res* 2003; **31**: 3812–3814.
11 Sunyaev S, Ramensky V, Koch I, Lathe 3rd W, Kondrashov AS, Bork P: Prediction of deleterious human alleles. *Hum Mol Genet* 2001; **10**: 591–597.

Supplementary Information accompanies the paper on European Journal of Human Genetics website (http://www.nature.com/ejhg)

CLINICAL GENETICS An International Journal of Genetics, Molecular and Personalized Medicine

Clin Genet 2011
Printed in Singapore. All rights reserved

CLINICAL GENETICS
doi: 10.1111/j.1399-0004.2011.01733.x

Letter to the Editor

Association of genomic deletions in the *STXBP1* gene with Ohtahara syndrome

To the Editor:

Ohtahara syndrome (OS) is characterized by early-onset of seizures, suppression-burst patterns on electroencephalogram (EEG), and severe psychomotor retardation (1–3). *De novo* mutations in the *STXBP1* gene, including various point mutations and one complete deletion, have been found in about one-third of Japanese cases of cryptogenic OS (4–6). However, the clinical spectrum of *STXBP1* mutations can be applied to other pathologies. For instance, in one study, *STXBP1* abnormalities including a microdeletion were detected in approximately 10% of patients (5/49) with early-onset epileptic encephalopathy that did not fit into a specific epilepsy syndrome (7). Other studies have also detected *de novo STXBP1* mutations in 2 of 95 individuals with mental retardation and non-syndromic epilepsy (8), in addition to the detection of a *de novo* partial deletion in a child with epilepsy and autistic features (9, 10). On the basis of these findings, extensive genetic testing including copy number analysis of *STXBP1* should be considered in children with early-onset seizures. However, the use of high-resolution copy number analysis of *STXBP1* thus far has been limited.

In this study, we performed customized array comparative genomic hybridization (aCGH) analysis, in which a total of 27,026 probes covering the *STXBP1* locus (UCSC coordinates, May 2006: Chr9: 129,350,808–129,558,072 bp) were distributed with 5-bp spacing except for repeating element regions (Roche NimbleGen, Tokyo, Japan). Among the 28 patients with cryptogenic OS tested, we found pathogenic *de novo* deletions in two patients (7.1%), where one 4.6-kb deletion included only exon 4, and the other 2.85-Mb one involved the entire *STXBP1* gene (Table 1).

Patient 1506, a product of unrelated healthy parents, had no problems in the perinatal period. Tonic seizures with a flexion of the upper extremities started at 32 days of age, and frequent myoclonic seizures subsequently appeared. On the basis of suppression-burst pattern on EEG, the patient was diagnosed as having OS or early myoclonic encephalopathy (EME), which is another epileptic syndrome showing suppression-burst pattern on EEG (11). As OS and EME have common features, they can be difficult to distinguish (2, 3). Brain magnetic resonance imaging (MRI) revealed normal neuroanatomy. High-dose phenobarbital was able to effectively reduce the frequency of seizures. Customized aCGH and breakpoint polymerase chain reaction (PCR) analyses detected a *de novo* 4635-bp deletion involving exon 4 of the *STXBP1* gene (Fig. 1a–c). The presence of a 2-bp microhomology at the deletion junction suggested non-homologous recombination leading to a

Table 1. Copy number alterations found in OS patients

	Findings of customized aCGH and 2.7M array (upper)/sequence-confirmed rearrangements (lower)						
Patient	Aberrations	Start (bp)	End (bp)	Size (bp)	Genes	Inheritance	Origin
1506	Deletion	129,457,591	129,462,084	4493	*STXBP1*(Ex4)	*De novo*	Unknown[a]
		129,457,463	129,462,098	4635	—	—	—
2231	Deletion	129,020,847	131,869,806	2,848,959	70 RefSeq genes including *STXBP* and *SPTAN1*	*De novo*	Paternal[b]
		129,020,309	131,870,400	2,850,091		—	—

aCGH, array comparative genomic hybridization; OS, Ohtahara syndrome.
[a]No informative markers were available within the 4.6-kb region corresponding to the deletion.
[b]Examined by the *D9S918* (UCSC coordinates, May 2006: Chr9: 129,497,050–129,497,376 bp) microsatellite marker.

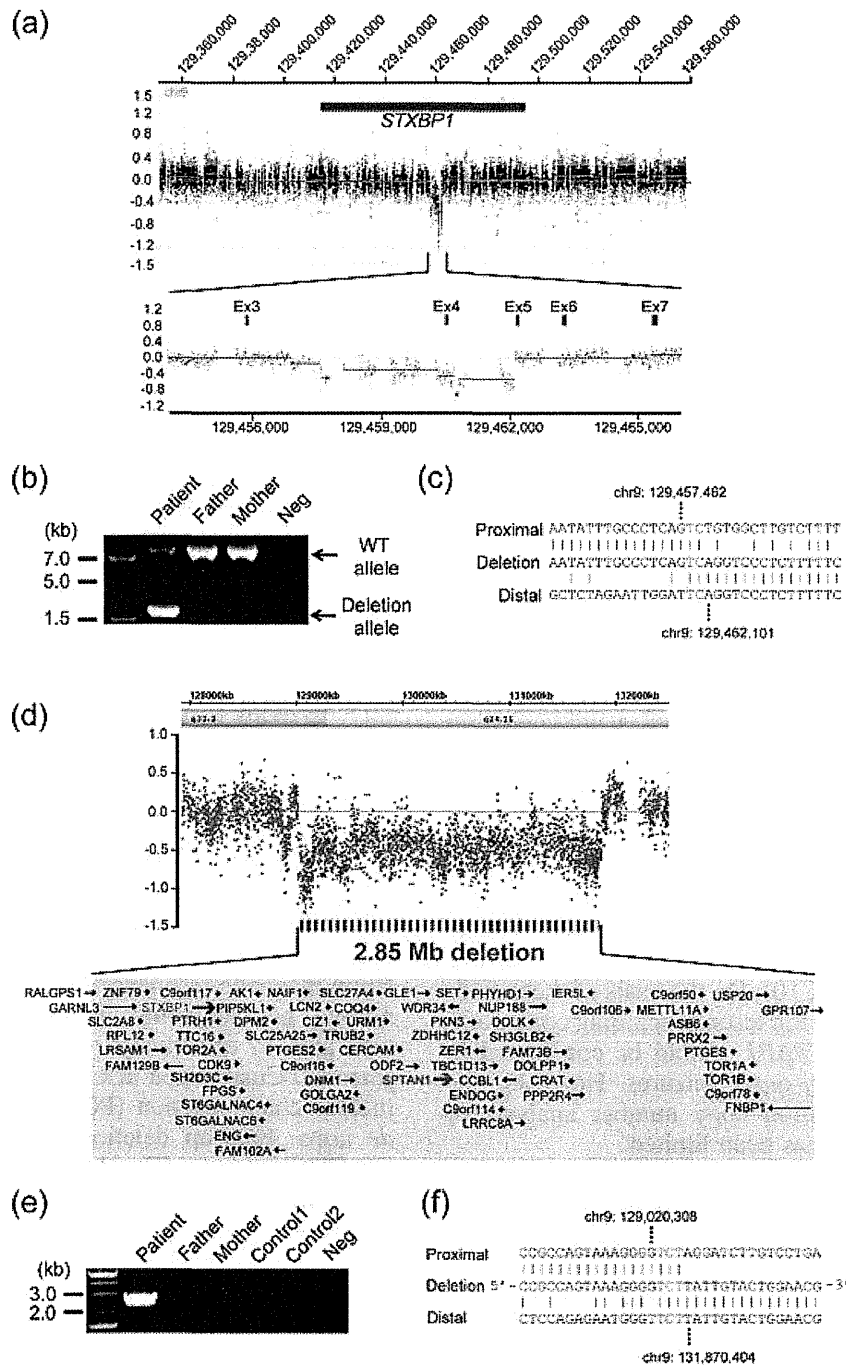

Fig. 1. The detection of two microdeletions using microarray. (**a**) A customized array comparative genomic hybridization (aCGH) profile of *STXBP1* locus in patient 1506. *x*- and *y*-axis show the genomic location from the p telomere of chromosome 9 (UCSC coordinates, May, 2006) and $\log_2$ (Cy3/Cy5 signal ratio) values (green dots ≥ 0.25; $-0.25 <$ black dots < 0.25; red dots ≤ -0.25), respectively (top panel). A close up view of the aCGH profile along with maps of the *STXBP1* exons (blue rectangles), showing the deletion of exon 4 (bottom panel). (**b**) Polymerase chain reaction (PCR) analysis of the family of patient 1506. Primers flanking the deletion amplified both 6398- and 1763-bp products from the wild type and deletion alleles, respectively, of the patient. However, the patient's parents had only a 6398-bp product, indicating the presence of a *de novo* deletion (Neg, negative control which contained no template DNA). (**c**) The deletion junction sequence. The top, middle and bottom strands show the proximal, deleted, and distal sequences, respectively. The two overlapping nucleotides are colored in red. (**d**) The 2.7M array profile clearly showed a 2.85-Mb deletion at 9q33.3-34.11 found in patient 2231 (top panel). A total of 70 RefSeq genes, including *STXBP1* and *SPTAN1*, were mapped within the deletion (bottom panel). (**e**) The breakpoint PCR analysis of the family of patient 2231. Primers flanking the deletion successfully amplified a 2430-bp product from the patient, indicating that the deletion occurred *de novo* (Neg, negative control that contained no template DNA). (**f**) The deletion junction sequence. The top, middle and bottom strands show the proximal, deleted and distal sequences, respectively. The three overlapping nucleotides are colored in red. The PCR conditions and primer sequences are available on request.

rearrangement (Fig. 1c) (12). The deletion of exon 4 was also confirmed by reverse transcriptase-PCR (Fig. S1, Supporting Information).

Patient 2231 was born at term after *in vitro* fertilization and embryo transfer. The body weight at birth was 2134 g (−2.4 SD), height 44.5 cm (−2.3 SD), and head circumference 32.0 cm (−0.8 SD). Multiple anomalies including cleft lip and palate, ventricular septal defect, overlapping fingers, and small penis were noted. G-banded chromosomal analysis was normal. The patient had an onset of sudden crying at 1 week of age followed by a cluster of epileptic spasms with suppression-burst pattern on EEG at 1 month. A brain MRI at 2 months showed a thin corpus callosum and relatively small cerebellum. After treatment with antiepileptic drugs proved ineffective, a ketogenic diet reduced the frequency of seizures. At 19 months, he showed spastic quadriplegia and profound intellectual disability at the level of a 2-month old. Customized aCGH, subsequent whole-genome 2.7M Array (Affymetrix, Santa Clara, CA), and breakpoint PCR analyses found a *de novo* 2.85-Mb microdeletion including *STXBP1* and *SPTAN1* (13) (Fig. 1d–f). The presence of a 3-bp homology at the deletion junction further suggested non-homologous recombination leading to the rearrangement (Fig. 1f).

In conclusion, our high-resolution copy number analysis in *STXBP1* locus revealed a 4.6-kb deletion encompassing only exon 4, which strongly suggests that copy number analysis covering all *STXBP1* exons should be recommended as a genetic test for children with early-onset seizures.

Supporting Information

The following Supporting information is available for this article:

Fig. S1. Examination of the mutated transcripts in lymphoblastoid cell lines derived from the patient 1506. (**a**) Reverse transcriptase polymerase chain reaction (RT-PCR) analysis of the patient with an exon 4 deletion relative to a normal control. A schematic representation of the transcript from exons 3 to 6 of *STXBP1* is indicated (top). The exons and primers are depicted as boxes and arrows, respectively. Two PCR products were amplified from the patient's cDNA: the upper was a wild-type (WT) transcript and the lower was the deleted mutant (middle). Only a single WT amplicon was detected in the control. The mutant amplicon was significantly increased by 30 μM cycloheximide (CHX) treatment for 4 h compared to dimethyl sulfoxide treatment as a vehicle control. RT (+): with reverse transcriptase, RT (−): without reverse transcriptase as a negative control. The sequence of the smaller amplicon clearly demonstrated exon 4 deletion (bottom). (**b**) Quantitative analysis of the nonsense-mediated mRNA decay (NMD) inhibition by CHX based on the data shown in (**a**). *p = 0.0023 by unpaired two tailed Student's *t*-test. Averages of duplicated experiments using two distinctive RNA samples are shown with error bars (SD). The mutant transcript lacking exon 4 created a premature stop codon at position 64, and suffered from degradation by NMD in the patient's lymphoblastoid cells. PCR conditions and the primer sequences are available on request.

Additional Supporting information may be found in the online version of this article.

Please note: Wiley-Blackwell Publishing is not responsible for the content or functionality of any supplementary materials supplied by the authors. Any queries (other than missing material) should be directed to the corresponding author for the article.

Acknowledgements

We would like to thank the patients and their families for their participation in this study. This work was supported by Research Grants from the Ministry of Health, Labour and Welfare (H. S., M. K., N. M. and N. M.), a Grant-in-Aid for Scientific Research from the Japan Society for the Promotion of Science (M. K. and N. M.), a Grant-in-Aid for Young Scientist from Japan Society for the Promotion of Science (H. S.), Research Promotion Fund from Yokohama Foundation for Advancement of Medical Science (H. S.), Research Grants from the Japan Epilepsy Research Foundation (H. S. and M. K.), and a Research Grant from Naito Foundation (N. M.).

H Saitsu[a]* *M Kato*[b]* *M Shimono*[c] *A Senju*[d] *S Tanabe*[d] *T Kimura*[d] *K Nishiyama*[a] *Y Yoneda*[a] *Y Kondo*[a] *Y Tsurusaki*[a] *H Doi*[a] *N Miyake*[a] *K Hayasaka*[b] *N Matsumoto*[a]

[a]Department of Human Genetics, Yokohama City University Graduate School of Medicine, Yokohama, Japan,

[b]Department of Pediatrics, Yamagata University Faculty of Medicine, Yamagata, Japan,

[c]Department of Pediatrics, School of Medicine, University of Occupational and Environmental Health, Kitakyushu, Japan, and

[d]Department of Pediatrics, Nihonkai General Hospital, Sakata, Japan

*These two authors contributed equally to this work.

References

1. Ohtahara S, Ishida T, Oka E et al. On the specific age dependent epileptic syndrome: the early-infantile epileptic encephalopathy with suppression-burst. No to Hattatsu 1976: 8: 270–279.
2. Djukic A, Lado FA, Shinnar S, Moshe SL. Are early myoclonic encephalopathy (EME) and the Ohtahara syndrome (EIEE) independent of each other? Epilepsy Res 2006: 70 (Suppl. 1): S68–S76.
3. Ohtahara S, Yamatogi Y. Ohtahara syndrome: with special reference to its developmental aspects for differentiating from early myoclonic encephalopathy. Epilepsy Res 2006: 70 (Suppl. 1): S58–S67.
4. Saitsu H, Kato M, Mizuguchi T et al. *De novo* mutations in the gene encoding STXBP1 (MUNC18-1) cause early infantile epileptic encephalopathy. Nat Genet 2008: 40: 782–788.
5. Saitsu H, Kato M, Okada I et al. *STXBP1* mutations in early infantile epileptic encephalopathy with suppression-burst pattern. Epilepsia 2010: 51: 2397–2405.
6. Saitsu H, Hoshino H, Kato M et al. Paternal mosaicism of an *STXBP1* mutation in OS. Clin Genet 2010. Epub ahead of print. DOI: 10.1111/j.1399-0004.2010.01575.x.

7. Deprez L, Weckhuysen S, Holmgren P et al. Clinical spectrum of early-onset epileptic encephalopathies associated with *STXBP1* mutations. Neurology 2010: 75: 1159–1165.
8. Hamdan FF, Piton A, Gauthier J et al. De novo *STXBP1* mutations in mental retardation and nonsyndromic epilepsy. Ann Neurol 2009: 65: 748–753.
9. Moretti P, Sahoo T, Hyland K et al. Cerebral folate deficiency with developmental delay, autism, and response to folinic acid. Neurology 2005: 64: 1088–1090.
10. Boone PM, Bacino CA, Shaw CA et al. Detection of clinically relevant exonic copy-number changes by array CGH. Hum Mutat 2010: 31: 1326–1342.
11. Engel J Jr. Report of the ILAE classification core group. Epilepsia 2006: 47: 1558–1568.
12. Lieber MR. The mechanism of double-strand DNA break repair by the nonhomologous DNA end-joining pathway. Annu Rev Biochem 2010: 79: 181–211.
13. Saitsu H, Tohyama J, Kumada T et al. Dominant-negative mutations in alpha-II spectrin cause West syndrome with severe cerebral hypomyelination, spastic quadriplegia, and developmental delay. Am J Hum Genet 2010: 86: 881–891.

Correspondence:
Dr Hirotomo Saitsu
Department of Human Genetics
Yokohama City University Graduate School of Medicine
3-9 Fukuura, Kanazawa-ku
Yokohama 236-0004
Japan
Tel.: +81 45 787 2606
Fax: +81 45 786 5219
e-mail: hsaitsu@yokohama-cu.ac.jp

CLINICAL REPORT

AMERICAN JOURNAL OF medical genetics PART A

De Novo 5q14.3 Translocation 121.5-kb Upstream of *MEF2C* in a Patient With Severe Intellectual Disability and Early-Onset Epileptic Encephalopathy

Hirotomo Saitsu,[1]* Noboru Igarashi,[2] Mitsuhiro Kato,[3] Ippei Okada,[1] Tomoki Kosho,[4] Osamu Shimokawa,[5] Yuki Sasaki,[5] Kiyomi Nishiyama,[1] Yoshinori Tsurusaki,[1] Hiroshi Doi,[1] Noriko Miyake,[1] Naoki Harada,[5] Kiyoshi Hayasaka,[3] and Naomichi Matasumoto[1]

[1]Department of Human Genetics, Yokohama City University Graduate School of Medicine, Yokohama, Japan

[2]Department of Pediatrics, Toyama Prefectural Central Hospital, Toyama, Japan

[3]Department of Pediatrics, Yamagata University Faculty of Medicine, Yamagata, Japan

[4]Department of Medical Genetics, Shinshu University School of Medicine, Matsumoto, Japan

[5]Cytogenetic Testing Group B, Advanced Medical Science Research Center, Mitsubishi Chemical Medience Corporation, Nagasaki, Japan

Received 2 March 2011; Accepted 27 June 2011

Recent studies have shown that haploinsufficiency of *MEF2C* causes severe intellectual disability, epilepsy, hypotonia, and cerebral malformations. We report on a female patient with severe intellectual disability, early-onset epileptic encephalopathy, and hypoplastic corpus callosum, possessing a de novo balanced translocation, t(5;15)(q13.3;q26.1). The patient showed upward gazing and tonic seizure of lower extremities followed by generalized clonic seizures at 4 months of age. Electroencephalogram showed hypsarrhythmia when asleep. By using fluorescent in situ hybridization (FISH), southern hybridization and inverse PCR, the translocation breakpoints were determined at the nucleotide level. The 5q14.3 breakpoint was localized 121.5-kb upstream of *MEF2C*. The 15q26.2 breakpoint was mapped 119-kb downstream of *LOC91948* non-coding RNA. We speculate that the translocation may disrupt the proper regulation of *MEF2C* expression in the developing brain, resulting in severe intellectual disability and early-onset epileptic encephalopathy.

Key words: *MEF2C*; early-onset epileptic encephalopathy; chromosomal translocation; regulatory region

How to Cite this Article:
Saitsu H, Igarashi N, Kato M, Okada I, Kosho T, Shimokawa O, Sasaki Y, Nishiyama K, Tsurusaki Y, Doi H, Miyake N, Harada N, Hayasaka K, Matsumoto N. 2011. De novo 5q14.3 translocation 121.5-kb upstream of *MEF2C* in a patient with severe intellectual disability and early-onset epileptic encephalopathy.
Am J Med Genet Part A 155:2879–2884.

INTRODUCTION

Early-onset epileptic encephalopathies, onset before 1 year of age, are characterized by severe seizures (often infantile spasms), frequent interictal epileptiform activity on a disorganized electroencephalogram (EEG) background, developmental regression, or retardation [Holland and Hallinan, 2010]. Ohtahara syndrome (OS), West syndrome, early myoclonic epileptic encephalopathy (EME), migrating partial seizures of infancy, and Dravet syndrome are the most well-known epileptic encephalopathies recognized by the International League Against Epilepsy (ILAE). However, many infants with these disorders do not strictly fit into the electroclinical parameters of these encephalopathies. Brain malformations and metabolic disorders were found as underlying causes of these syndromes, but a significant portion of idiopathic or cryptogenic cases remains etiologically unexplained. Recently, several causative genes have been reported: *ARX* in the OS and West syndrome phenotypes, *CDKL5* in West syndrome, *STXBP1* in OS, *SLC25A22*

Additional supporting information may be found in the online version of this article.

Grant sponsor: Ministry of Health, Labour and Welfare; Grant sponsor: Japan Society for the Promotion of Science; Grant sponsor: Yokohama Foundation for Advancement of Medical Science; Grant sponsor: Japan Epilepsy Research Foundation; Grant sponsor: Naito Foundation.
*Correspondence to:
Hirotomo Saitsu, M.D., Ph.D., Department of Human Genetics, Yokohama City University Graduate School of Medicine, 3-9 Fukuura, Kanazawa-ku, Yokohama 236-0004, Japan.
E-mail: hsaitsu@yokohama-cu.ac.jp
Published online 11 October 2011 in Wiley Online Library (wileyonlinelibrary.com).
DOI 10.1002/ajmg.a.34289

in EME, *SCN1A* in Dravet syndrome [Claes et al., 2001; Stromme et al., 2002; Kalscheuer et al., 2003; Molinari et al., 2005; Kato et al., 2007; Saitsu et al., 2008]. Identification of new causative genes is absolutely necessary for further understanding of infantile epileptic syndromes.

Microdeletions at 15q14.3 encompassing the *myocyte enhancer-binding factor 2C* (*MEF2C*) gene has been recently reported in patients with severe intellectual disability (ID), epilepsy often starting in infancy, hypotonia, and cerebral malformations [Cardoso et al., 2009; Engels et al., 2009; Le Meur et al., 2010]. Identification of five de novo mutations (three truncating and two missense ones) in *MEF2C* and a deletion only involving *MEF2C* in patients with similar phenotype clearly demonstrated that haploinsufficiency of *MEF2C* is responsible for these features [Le Meur et al., 2010; Novara et al., 2010; Nowakowska et al., 2010; Zweier et al., 2010]. Various kinds of seizures were observed in these patients with *MEF2C* abnormalities, including infantile spasm, and myoclonic, tonic-clonic, and febrile seizures [Le Meur et al., 2010; Novara et al., 2010; Nowakowska et al., 2010; Zweier et al., 2010]. Interstingly, a 3.57-Mb microdeletion 233.3-kb upstream of *MEF2C* resulted in significant loss of *MEF2C* expression in a patient with severe ID, hypotonia, epilepsy, and stereotypic hand movements [Zweier et al., 2010]. Moreover, a de novo balanced translocation, t(5;8)(q14.3;q23.3), in a patient with ID, epilepsy, and stereotypic movements has been reported, showing that the 5q14.3 breakpoint was located approximately 500-kb upstream of *MEF2C* [Floris et al., 2008]. All of these reports support the importance of upstream regulatory regions in controlling *MEF2C* expression.

Here, we report on a patient with severe intellectual disability and early-onset epileptic encephalopathy as well as a de novo balanced translocation, t(5;15)(q13.3;q26.1), which turned out related to *MEF2C*. Detailed genomic analysis is presented.

CLINICAL REPORT

The 7-year-old girl is a product of unrelated healthy parents. She was born at term without asphyxia after uneventful pregnancy. Body weight at birth was 2,584 g (−1.1 SD), height 47.0 cm (−1.0 SD), and head circumference 31.0 cm (−1.6 SD). Poor visual contact and nystagmus were noticed at 3 months of age. Ophthalmic examinations were unremarkable. Upward gazing and tonic seizures of lower extremities followed by generalized clonic seizures were observed at 3 months of age. EEG showed hypsarrhythmia when asleep (Fig. 1A). Seizures, which were observed as many as 40 times a day, were transiently controlled by combination of valproic acid, adrenocorticotropic hormone administration, and clobazam. Cerebral blood flow examination revealed low perfusion at right frontal area. Brain magnetic resonance imaging (MRI) showed reduced volume of white matter and normal cortical brain structure except for hypoplastic corpus callosum, especially in genu and splenium (Fig. 1B,C).

Profound intellectual disability and developmental delay ensued. The patient showed spastic quadriplegia, but no hypotonia. She could not walk or speak a word. Eye contact was poor. She could neither sit alone nor turnover, and required total care. She showed gastroesophageal reflux and was tube-fed. She did not exhibit stereotypic movements. The EEG at the age of 4 years showed irregular high-voltage slow wave activity intermingled with fast wave. At present, her weight was 11.5 kg (−2.7 SD), height 108 cm (−2.5 SD), and head circumference 45.0 cm (−4.8 SD). She had severe deformity of trunk and extremities. Brief tonic seizures with blinking were observed several times a day despite administration of antiepilepstic drugs (valproic acid, clobazam, and zonisamide). In infancy, she had a square face with short palpebral fissures, a short and depressed nose with anteverted nostrils, a tented vermilion of the upper lip, and a protruded tongue. In childhood, her face became round and flat. The tented vermillion of upper lip might be shared by the patient and several patients with *MEF2C* abnormalities.

MATERIALS AND METHODS

Molecular Cytogenetic Analysis

G-banded chromosomes of peripheral blood lymphocytes were analyzed. Fluorescence in situ hybridization (FISH) was performed on fixed peripheral lymphocytes. Labeling, hybridization, wash, and image acquisition were performed as previously described [Saitsu et al., 2008]. RPCI-11 BAC clones and approximately 15-kb probes amplified by long PCR using KOD-FX polymerase (Toyobo, Osaka, Japan) using RP11-634n8 DNA as a template were used as probes. Primer information is shown in the Supplemental eTable available online in Supporting Information.

Affymetrix Cytogenetics Whole-Genome 2.7M Array

Copy number alterations were studied by Cytogenetics Whole-Genome 2.7M Array (Affymetrix, Santa Clara, CA). Experimental procedures were performed according to the manufacturer's protocol. Copy number alterations were analyzed by Chromosome Analysis Suite (ChAS; Affymetrix) with NA30.1 (hg18) annotations.

Cloning of Translocation Breakpoints

The 5q14.3 translocation breakpoint was analyzed by Southern hybridization using *Bgl*II- and *Sac*I-digested patient DNA. Mother's DNA was used as a control. Probes were synthesized by PCR DIG probe synthesis kit (Roche, Basel, Switzerland) using RP11-634n8 DNA as a template. Hybridization, washing, and detection of probes were done according to the manufacturer's protocol. Images were captured on FluorChem (Alpha Innotech, San Leandro, CA). To obtain the der(5) translocation junction fragment, *Sac*I-digested DNA of the patient was self-ligated by Ligation high Ver.2 (Toyobo), ethanol precipitated and dissolved in 20 μl EB buffer (Qiagen, Tokyo, Japan). Inverse PCR was performed in 25 μl of volume, containing 2 μl ligated DNA, 1× PCR Buffer for KOD FX, 0.4 mM each dNTP, 0.3 μM each primer, and 0.3 U KOD FX polymerase (Toyobo). Negative controls only used either forward or reverse primer. The PCR product was electrophoresed in 0.7% agarose gel, and the aberrant band corresponding to der(5) fragment was purified by QIAquick Gel Extraction Kit (Qiagen). The purified DNA was sequenced for both forward and reverse

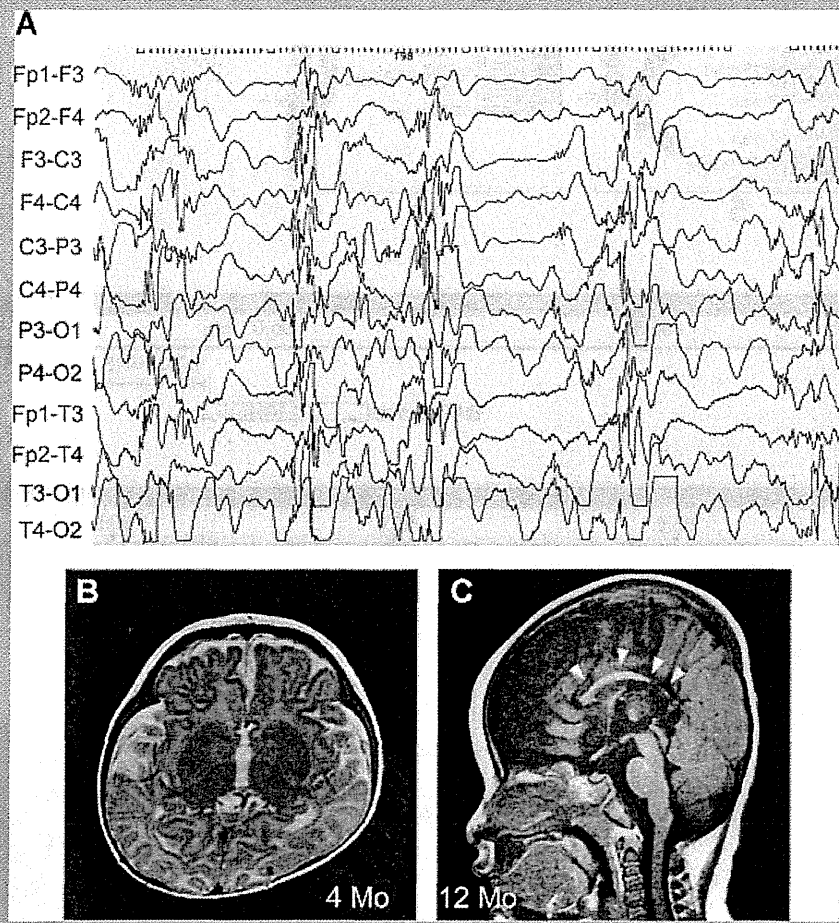

FIG. 1. EEG and brain MRI in the patient. A: Interictal sleep EEG at 4 months demonstrated diffuse or multifocal polyspikes or sharp waves concomitant with irregular high-voltage slow wave. Desynchronization lasting for 1–2 sec can also be seen predominantly in bilateral frontal area. B,C: Brain MRI of the patient at age of 4 months (B) and 12 months (C). T2-weighted axial (B) and T1-weighted sagittal (C) images showed normal cortical brain structure except for hypoplastic corpus callosum (arrowheads), especially in genu and splenium.

strands with BigDye Terminator chemistry ver. 3 according to the standard protocol (Applied Biosystems, Foster city, CA). After identification of breakpoint sequences of der(5), breakpoint-specific primers for both der(5) and der(15) translocation junctions were designed. Junction fragments were amplified by PCR using these primer-sets on DNAs of the patient and her parents. Primer information is shown in the Supplemental eTable available online in Supporting Information.

RESULTS

G-banded chromosomal analysis revealed a balanced translocation t(5;15)(q13.3;q26.1) (Fig. 2A). Her parents showed a normal karyotype (data not shown), indicating that the translocation occurred de novo. Subsequent FISH analysis demonstrated that the breakpoints in chromosome 5 and 15 were covered by the clones RP11-690g22 and 634n8, and 1061g3, respectively, indicating that the translocation did not directly disrupt any genes (Fig. 2B–D). Interestingly, the breakpoint on 5q14.3 was located near the *MEF2C* gene, a causative gene for severe ID, epilepsy, and cerebral malformations [Cardoso et al., 2009; Engels et al., 2009; Le Meur et al., 2010; Novara et al., 2010; Nowakowska et al., 2010; Zweier et al., 2010]. The breakpoint on 5q14.3 was further narrowed down by FISH analysis using long PCR products as probes (Fig. 2C). Probe II showed weak but clear signals on chromosome 5, and derivative chromosomes 5 and 15, suggesting that the breakpoint was located within the probe II (data not shown). Southern hybridization analysis using probes P1 and P2 detected different aberrant bands only in the patient (Fig. 2C,E), indicating that the breakpoint was located at the region between the two probes. Inverse PCR on *Sac*I-digested DNA was successful in obtaining a der(5) breakpoint-junction fragment. Sequence analysis showed that the 5q14.3 breakpoint was located 121.5-kb upstream of the transcription start site of *MEF2C* (isoform 1, NM_002397.3) (Fig. 2C,F). Breakpoint-specific PCR analysis of the patient and her parents confirmed that the rearrangements occurred de novo (Fig. 2G). The

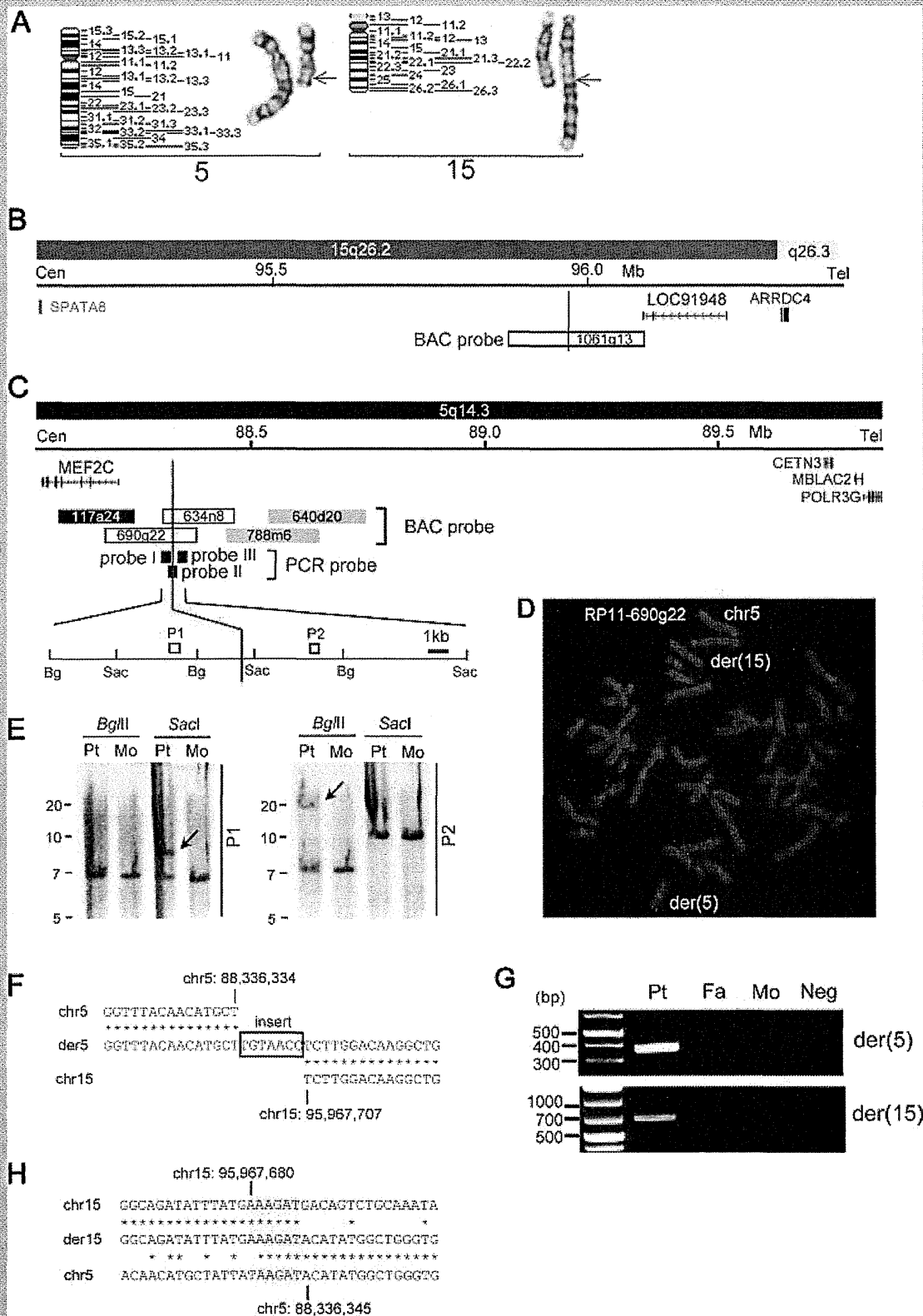
A
5
15
B
15q26.2
q26.3
Cen
95.5
96.0 Mb
Tel
SPATA8
LOC91948
ARRDC4
BAC probe
1051g13
C
5q14.3
Cen
88.5
89.0
89.5 Mb
Tel
MEF2C
CETN3
MBLAC2
POLR3G
117a24
634n8
640d20
690g22
788m6
BAC probe
probe I
probe III
probe II
PCR probe
P1
P2
1kb
Bg
Sac
Bg
Sac
Bg
Sac
D
RP11-690g22
chr5
der(15)
der(5)
E
BglII
SacI
Pt
Mo
Pt
Mo
20
10
7
5
P1
P2
F
chr5: 88,336,334
chr5
GGTTTACAACATGCT
insert
der5
GGTTTACAACATGCT
TCTTGGACAAGGCTG
chr15
TCTTGGACAAGGCTG
chr15: 95,967,707
G
(bp)
Pt
Fa
Mo
Neg
500
400
300
der(5)
1000
700
500
der(15)
H
chr15: 95,967,680
chr15
GGCAGATATTTATGAAAGATGACAGTCTGCAAATA
der15
GGCAGATATTTATGAAAGATACATATGGCTGGGTG
chr5
ACAACATGCTATTATAAAGATACATATGGCTGGGTG
chr5: 88,336,345

FIG. 2.

15q26.2 breakpoint was determined at the nucleotide level by sequencing of the beakpoint-specific PCR fragment (Fig. 1H). It was located 119-kb downstream of *LOC91948* non-coding RNA (Fig. 2B). To check genomic copy number alterations accompanied by the rearrangement, Cytogenetics Whole-Genome 2.7M Array (Affymetrix, Santa Clara, CA) was performed. Besides five known copy number variations, no other imbalances were detected (data not shown).

DISCUSSION

Expression of the members of MEF2 family transcription factors (*MEFA-D*) in the developing brain, which belong to the MADS (MCMl-agamous-deficiens-serum response factor) superfamily of DNA-binding proteins, shows spaciotemporal patterns correlating with withdrawal from the cell cycle and initiation of neuronal differentiation [Lyons et al., 1995]. After mouse *Mef2c* is first expressed in developing brain at embryonic day 11.5, *Mef2c* is highly expressed in cerebral cortex, hippocampus, amygdala, thalamus, midbrain, and Purukinje cells in the adult brain [Lyons et al., 1995]. It has recently reported that two independent conditional knockout lines of *Mef2c*, which resulted in deletion of *Mef2c* in neural stem/progenitor cells (NSCs), showed significant neurological deficits. One line with deletion of *Mef2c* in NSCs later in development showed impairment of hippocampal-dependent learning and memory, suggesting that *Mef2c* can limt excessive synapse formation during activity-dependent refinement of synaptic connectivity [Barbosa et al., 2008]. Of note, deletion of *Mef2c* in NSCs earlier in development resulted in severe behavioral deficits reminiscent of Rett syndrome [Li et al., 2008]. The mice also exhibited fewer, smaller, and more compacted neurons, similar to findings in Rett syndrome [Li et al., 2008]. In humans, *MEF2C* mutation/deletion cause severe ID, epilepsy, hypotonia, and cerebral malformations [Engels et al., 2009; Le Meur et al., 2010; Novara et al., 2010; Nowakowska et al., 2010; Zweier et al., 2010]. In addition, some patients showed repetitive clapping movements like Rett syndrome [Le Meur et al., 2010]. Considering essential roles of *MEF2C* in brain development both in humans and mice, the precise control of *MEF2C* expression should be very important.

In our patient, the 5q14.3 breakpoint was located 121.5-kb upstream of *MEF2C*. Two previous reports suggested that genomic regions 233- to 500-kb upstream of *MEF2C* may be required for proper *MEF2C* expression: a 3.57-Mb microdeletion 233.3-kb upstream of *MEF2C* resulted in significant loss of *MEF2C* expression [Zweier et al., 2010], and a de novo balanced translocation located approximately 500-kb upstream of *MEF2C* was associated with ID, epilepsy, and stereotypic movements similar to *MEF2C* mutation/deletion [Floris et al., 2008]. Thus, it is likely that the translocation may disrupt regulation of *MEF2C* expression in the developing brain. However, we did not observe any significant decrease of *MEF2C* expression in lymphoblastoide cells derived from the patient (data not shown). It has been reported that *MEF2C* expression in blood cells was significantly decreased in all patients with either a microdeletion or a truncating mutation [Zweier et al., 2010]. We speculate that the 5q14.3 translocation may alter proper *MEF2C* expression in the developing brain of the patient analyzed here.

The patient showed severe ID, early-onset epileptic encephalopathy. Brain MRI showed hypoplastic corpus callosum, especially in genu and splenium. All the three features (severe ID, seizure, and cerebral malformation) are common in patients with the *MEF2C* mutation/deletion. By contrast, our patient showed spastic quadriplegia, but not muscluar hypotonia which is common in approximately 90% of patients with *MEF2C* mutation/deletion (19/21) [Engels et al., 2009; Le Meur et al., 2010; Novara et al., 2010; Nowakowska et al., 2010; Zweier et al., 2010]. Thus, our patient may be an atypical case of *MEF2C* abnormality, probably due to unusual *MEF2C* expression in the brain caused by the 5q14.3 translocation.

In conclusion, we described a patient with severe ID, early-onset epileptic encephalopathy, and hypoplastic corpus callosum, carrying a de novo reciprocal translocation 121.5-kb upstream of *MEF2C*. Our report strengthens the role of *MEF2C* in severe ID with early-onset epileptic encephalopathy, and highlights importance of its upstream regulatory region.

FIG. 2. Genomic characterization of t(5;15)(q13.3;q26.1). A: Partial karyotype of the patient. Left shows chromosomes 5 (left: normal, right: derivative), and right shows chromosomes 15 (left: normal, right: derivative). B,C: Summarized physical maps covering the 15q26.2 (B) and 5q14.3 (C) translocation breakpoints. RP11-1061g13 spans the 15q26.2 breakpoint (B, red longitudinal line). RP11-690g22 and 634n8, and PCR probe II span the 5q14.3 breakpoint (C, red line). Note that the translocation did not directly disrupt any genes. More detailed maps are shown (C, bottom). A partial restriction map (Bg, *Bgl*II; Sac, *Sac*I), probes for Southern hybridization (P1, P2) are indicated. Translocation breakpoint (red line) is located between P1 and P2. D: FISH analysis using RP11-690g22 as a probe showed signals on chromosome 5, and der(5) and der(15) chromosomes. E: Southern hybridization using probes P1, and P2 on genomic DNA of the patient and her mother. Arrow shows aberrant bands specific to the patient (not observed in maternal DNA). Pt, patient; Mo, mother. F: Breakpoint junction sequences of der(5). Top, middle, and bottom sequence strands show normal 5, derivative 5, and normal 15 chromosomes, respectively. Breakpoint positions are marked with small longitudinal lines based on the UCSC genome browser coordinates (version March 2006). Asterisks indicate nucleotides identical to normal chromosomes. A small 7-bp nucleotide insertion was identified at the breakpoint (box). G: Breakpoint-specific PCR analysis of the patient's family. Primers specific to der(5) and der(15) breakpoints could successfully amplify 366- and 689-bp products, respectively, only from the patient (Pt), indicating the translocation occurred de novo. Fa, father; Mo, mother. H: Breakpoint junction sequences of der(15). Top, middle, and bottom sequence strands show normal 15, derivative 15, and normal 5 chromosomes, respectively. The five overlapping nucleotides (colored in red) are identified at the breakpoint.

ACKNOWLEDGMENTS

We would like to thank the patient and her family for their participation in this study. This work was supported by Research Grants from the Ministry of Health, Labour and Welfare (H.S., N. Matsumoto, N. Miyake, and M.K.), Grant-in-Aid for Scientific Research from Japan Society for the Promotion of Science (N. Matsumoto, N. Miyake and M.K.), Grant-in-Aid for Young Scientist from Japan Society for the Promotion of Science (H.S. and N. Miyake), Research Promotion Fund from Yokohama Foundation for Advancement of Medical Science (H.S.), Research Grants from the Japan Epilepsy Research Foundation (H.S. and M.K.), and Research Grant from Naito Foundation (N. Matsumoto).

REFERENCES

Barbosa AC, Kim MS, Ertunc M, Adachi M, Nelson ED, McAnally J, Richardson JA, Kavalali ET, Monteggia LM, Bassel-Duby R, Olson EN. 2008. MEF2C, a transcription factor that facilitates learning and memory by negative regulation of synapse numbers and function. Proc Natl Acad Sci USA 105:9391–9396.

Cardoso C, Boys A, Parrini E, Mignon-Ravix C, McMahon JM, Khantane S, Bertini E, Pallesi E, Missirian C, Zuffardi O, Novara F, Villard L, Giglio S, Chabrol B, Slater HR, Moncla A, Scheffer IE, Guerrini R. 2009. Periventricular heterotopia, mental retardation, and epilepsy associated with 5q14.3-q15 deletion. Neurology 72:784–792.

Claes L, Del-Favero J, Ceulemans B, Lagae L, Van Broeckhoven C, De Jonghe P. 2001. De novo mutations in the sodium-channel gene SCN1A cause severe myoclonic epilepsy of infancy. Am J Hum Genet 68: 1327–1332.

Engels H, Wohlleber E, Zink A, Hoyer J, Ludwig KU, Brockschmidt FF, Wieczorek D, Moog U, Hellmann-Mersch B, Weber RG, Willatt L, Kreiss-Nachtsheim M, Firth HV, Rauch A. 2009. A novel microdeletion syndrome involving 5q14.3-q15: Clinical and molecular cytogenetic characterization of three patients. Eur J Hum Genet 17:1592–1599.

Floris C, Rassu S, Boccone L, Gasperini D, Cao A, Crisponi L. 2008. Two patients with balanced translocations and autistic disorder: CSMD3 as a candidate gene for autism found in their common 8q23 breakpoint area. Eur J Hum Genet 16:696–704.

Holland KD, Hallinan BE. 2010. What causes epileptic encephalopathy in infancy?: The answer may lie in our genes. Neurology 75:1132–1133.

Kalscheuer VM, Tao J, Donnelly A, Hollway G, Schwinger E, Kubart S, Menzel C, Hoeltzenbein M, Tommerup N, Eyre H, Harbord M, Haan E, Sutherland GR, Ropers HH, Gecz J. 2003. Disruption of the serine/threonine kinase 9 gene causes severe X-linked infantile spasms and mental retardation. Am J Hum Genet 72:1401–1411.

Kato M, Saitoh S, Kamei A, Shiraishi H, Ueda Y, Akasaka M, Tohyama J, Akasaka N, Hayasaka K. 2007. A longer polyalanine expansion mutation in the ARX gene causes early infantile epileptic encephalopathy with suppression-burst pattern (Ohtahara syndrome). Am J Hum Genet 81: 361–366.

Le Meur N, Holder-Espinasse M, Jaillard S, Goldenberg A, Joriot S, Amati-Bonneau P, Guichet A, Barth M, Charollais A, Journel H, Auvin S, Boucher C, Kerckaert JP, David V, Manouvrier-Hanu S, Saugier-Veber P, Frebourg T, Dubourg C, Andrieux J, Bonneau D. 2010. MEF2C haploinsufficiency caused by either microdeletion of the 5q14.3 region or mutation is responsible for severe mental retardation with stereotypic movements, epilepsy and/or cerebral malformations. J Med Genet 47:22–29.

Li H, Radford JC, Ragusa MJ, Shea KL, McKercher SR, Zaremba JD, Soussou W, Nie Z, Kang YJ, Nakanishi N, Okamoto S, Roberts AJ, Schwarz JJ, Lipton SA. 2008. Transcription factor MEF2C influences neural stem/progenitor cell differentiation and maturation in vivo. Proc Natl Acad Sci USA 105:9397–9402.

Lyons GE, Micales BK, Schwarz J, Martin JF, Olson EN. 1995. Expression of mef2 genes in the mouse central nervous system suggests a role in neuronal maturation. J Neurosci 15:5727–5738.

Molinari F, Raas-Rothschild A, Rio M, Fiermonte G, Encha-Razavi F, Palmieri L, Palmieri F, Ben-Neriah Z, Kadhom N, Vekemans M, Attie-Bitach T, Munnich A, Rustin P, Colleaux L. 2005. Impaired mitochondrial glutamate transport in autosomal recessive neonatal myoclonic epilepsy. Am J Hum Genet 76:334–339.

Novara F, Beri S, Giorda R, Ortibus E, Nageshappa S, Darra F, Dalla Bernardina B, Zuffardi O, Van Esch H. 2010. Refining the phenotype associated with MEF2C haploinsufficiency. Clin Genet 78:471–477.

Nowakowska BA, Obersztyn E, Szymanska K, Bekiesinska-Figatowska M, Xia Z, Ricks CB, Bocian E, Stockton DW, Szczaluba K, Nawara M, Patel A, Scott DA, Cheung SW, Bohan TP, Stankiewicz P. 2010. Severe mental retardation, seizures, and hypotonia due to deletions of MEF2C. Am J Med Genet Part B 153B:1042–1051.

Saitsu H, Kato M, Mizuguchi T, Hamada K, Osaka H, Tohyama J, Uruno K, Kumada S, Nishiyama K, Nishimura A, Okada I, Yoshimura Y, Hirai S, Kumada T, Hayasaka K, Fukuda A, Ogata K, Matsumoto N. 2008. De novo mutations in the gene encoding STXBP1 (MUNC18-1) cause early infantile epileptic encephalopathy. Nat Genet 40:782–788.

Stromme P, Mangelsdorf ME, Shaw MA, Lower KM, Lewis SM, Bruyere H, Lutcherath V, Gedeon AK, Wallace RH, Scheffer IE, Turner G, Partington M, Frints SG, Fryns JP, Sutherland GR, Mulley JC, Gecz J. 2002. Mutations in the human ortholog of Aristaless cause X-linked mental retardation and epilepsy. Nat Genet 30:441–445.

Zweier M, Gregor A, Zweier C, Engels H, Sticht H, Wohlleber E, Bijlsma EK, Holder SE, Zenker M, Rossier E, Grasshoff U, Johnson DS, Robertson L, Firth HV, Ekici AB, Reis A, Rauch A. 2010. Mutations in MEF2C from the 5q14.3q15 microdeletion syndrome region are a frequent cause of severe mental retardation and diminish MECP2 and CDKL5 expression. Hum Mutat 31:722–733.

REPORT

Mutations in *POLR3A* and *POLR3B* Encoding RNA Polymerase III Subunits Cause an Autosomal-Recessive Hypomyelinating Leukoencephalopathy

Hirotomo Saitsu,[1,*] Hitoshi Osaka,[2] Masayuki Sasaki,[3] Jun-ichi Takanashi,[4] Keisuke Hamada,[5] Akio Yamashita,[6] Hidehiro Shibayama,[7] Masaaki Shiina,[5] Yukiko Kondo,[1] Kiyomi Nishiyama,[1] Yoshinori Tsurusaki,[1] Noriko Miyake,[1] Hiroshi Doi,[1] Kazuhiro Ogata,[5] Ken Inoue,[8] and Naomichi Matsumoto[1,*]

Congenital hypomyelinating disorders are a heterogeneous group of inherited leukoencephalopathies characterized by abnormal myelin formation. We have recently reported a hypomyelinating syndrome characterized by diffuse cerebral hypomyelination with cerebellar atrophy and hypoplasia of the corpus callosum (HCAHC). We performed whole-exome sequencing of three unrelated individuals with HCAHC and identified compound heterozygous mutations in *POLR3B* in two individuals. The mutations include a nonsense mutation, a splice-site mutation, and two missense mutations at evolutionally conserved amino acids. Using reverse transcription-PCR and sequencing, we demonstrated that the splice-site mutation caused deletion of exon 18 from *POLR3B* mRNA and that the transcript harboring the nonsense mutation underwent nonsense-mediated mRNA decay. We also identified compound heterozygous missense mutations in *POLR3A* in the remaining individual. *POLR3A* and *POLR3B* encode the largest and second largest subunits of RNA Polymerase III (Pol III), RPC1 and RPC2, respectively. RPC1 and RPC2 together form the active center of the polymerase and contribute to the catalytic activity of the polymerase. Pol III is involved in the transcription of small noncoding RNAs, such as 5S ribosomal RNA and all transfer RNAs (tRNA). We hypothesize that perturbation of Pol III target transcription, especially of tRNAs, could be a common pathological mechanism underlying *POLR3A* and *POLR3B* mutations.

Congenital hypomyelinating disorders form a heterogeneous group of central nervous system leukoencephalopathies that is characterized by abnormal myelin formation. Although these conditions are readily recognized by brain magnetic resonance imaging (MRI), many cases are not diagnosed correctly.[1] Several syndromes affecting myelination, such as hypomyelination with hypodontia and hypogonadotropic hypogonadism (4H) syndrome (MIM 612440) and hypomyelination with atrophy of the basal ganglia and cerebellum (H-ABC) (MIM 612438), have been described.[2–5] We have recently reported a hypomyelinating syndrome characterized by diffuse cerebral hypomyelination with cerebellar atrophy and hypoplasia of the corpus callosum (HCAHC).[6] Individuals with HCAHC do not show hypodontia or atrophy of the basal ganglia, which are observed in 4H syndrome and H-ABC; however, diffuse hypomyelination, atrophy, or hypoplasia of the cerebellum and corpus callosum are overlapping features of these three syndromes, suggesting that there might be a common underlying pathological mechanism.

Here, we report on four individuals with HCAHC from three unrelated families (Figure 1A; Table 1). Clinical information and peripheral blood or saliva samples were obtained from the family members after obtaining written informed consent. Experimental protocols were approved by the Institutional Review Board of Yokohama City University. To identify pathogenic mutations, we performed whole-exome sequencing of three probands from three unrelated families (individuals 1, 3, and 4). DNAs were captured with the SureSelect Human All Exon 50Mb Kit (Agilent Technologies, Santa Clara, CA) and sequenced with one lane per sample on an Illumina GAIIx (Illumina, San Diego, CA) with 108 bp paired-end reads. Image analysis and base calling were performed by sequence control software real-time analysis and CASAVA software v1.7 (Illumina). A total of 90,014,368 (individual 1), 86,942,264 (individual 3), and 92,168,758 (individual 4) paired-end reads were obtained and aligned to the human reference genome sequence (GRCh37/hg19) with MAQ[7] and NextGENe software v2.00 with sequence condensation by consolidation (SoftGenetics, State College, PA). This approach resulted in more than 88% of target exomes being covered by ten reads or more (see Table S1, available online). Single nucleotide variants (SNVs) were called with MAQ and NextGENe. Small insertions and deletions were

[1]Department of Human Genetics, Yokohama City University Graduate School of Medicine, 3-9 Fukuura, Kanazawa-ku, Yokohama 236-0004, Japan; [2]Division of Neurology, Clinical Research Institute, Kanagawa Children's Medical Center, 2-138-4 Mutsukawa, Minami-ku, Yokohama 232-8555, Japan; [3]Department of Child Neurology, National Center of Neurology and Psychiatry, 4-1-1 Ogawahigashi-cho Kodaira, Tokyo 187-8551, Japan; [4]Department of Pediatrics, Kameda Medical Center, 929 Higashi-cho, Kamogawa-shi, Chiba 296-8602, Japan; [5]Department of Biochemistry, Yokohama City University Graduate School of Medicine, 3-9 Fukuura, Kanazawa-ku, Yokohama 236-0004, Japan; [6]Department of Molecular Biology, Yokohama City University Graduate School of Medicine, 3-9 Fukuura, Kanazawa-ku, Yokohama 236-0004, Japan; [7]Department of Neurology, Kameda Medical Center, 929 Higashi-cho, Kamogawa-shi, Chiba 296-8602, Japan; [8]Department of Mental Retardation and Birth Defect Research, National Institute of Neuroscience, National Center of Neurology and Psychiatry, 4-1-1 Ogawahigashi-cho Kodaira, Tokyo 187-8551, Japan
*Correspondence: hsaitsu@yokohama-cu.ac.jp (H.S.), naomat@yokohama-cu.ac.jp (N.M.)
DOI 10.1016/j.ajhg.2011.10.003.

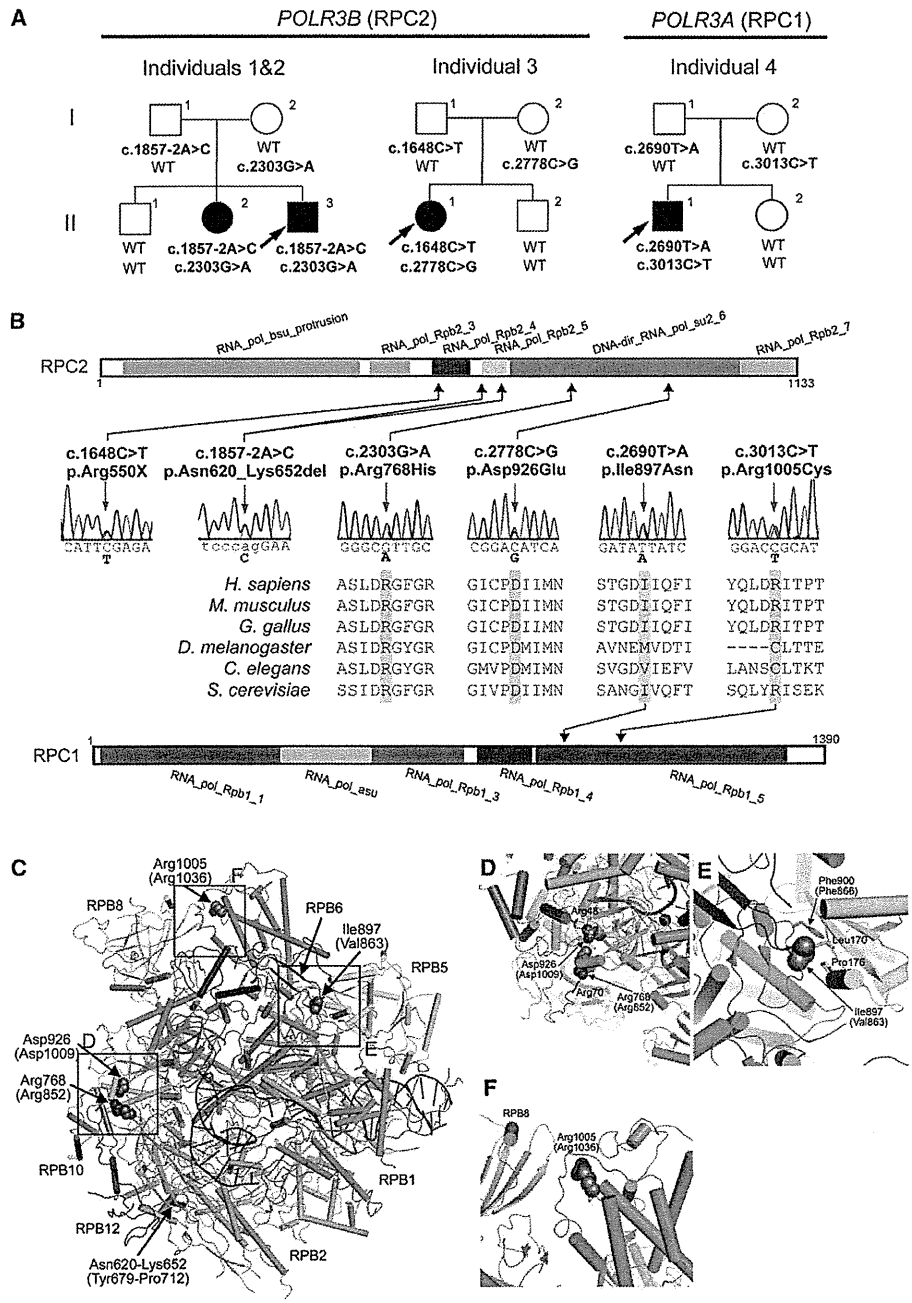

Figure 1. Mutations in *POLR3B* and *POLR3A*

(A) Pedigrees of four kindreds with HCAHC are shown. We identified four mutations in *POLR3B* encoding RPC2 in three individuals from two unrelated families and two mutations in *POLR3A* encoding RPC1 in one family. The segregation of each mutation is shown.

(B) Schematic representation of RPC2 (upper) and RPC1 (lower) proteins with Pfam domains (from Ensembl). Locations of each amino-acid-altering mutation are depicted with electropherograms. All of the missense mutations occurred at evolutionally conserved amino acids. Homologous sequences were aligned with the CLUSTALW website.

(C–F) 3D representations of RPC1 and RPC2 mutations. Mutated amino acids in RPC1 and RPC2 are shown along with their equivalent positions in the homologous RPB1 and RPB2 subunits of RNA Polymerase II (amino acid and its position in parenthesis). The structure and positions of mutations are illustrated by PyMOL with the crystal structure (PDB accession number 3GTP). RPB3, RPB9, and RPB11 subunits, which are specific to RNA Polymerase II, have been omitted from the figure. RPB1 is shown in green, RPB2 in sky blue, RPB5 in yellow, RPB6 in dark blue, RPB8 in pink, RPB10 in orange, RPB12 in purple, DNA in brown, and RNA in red. Amino acids that interact with mutated amino acids are also shown.

Table 1. Clinical Features of the Individuals

Clinical Features	Individual 1	Individual 2	Individual 3	Individual 4
Genes	*POLR3B*	*POLR3B*	*POLR3B*	*POLR3A*
Mutations, DNA	c.1857-2A>C, c.2303G>A	c.1857-2A>C, c.2303G>A	c.1648C>T, c.2778C>G	c.2690T>A, c.3013C>T
Mutations, protein	p.Asn620_Lys652del, p.Arg768His	p.Asn620_Lys652del, p.Arg768His	p.Arg550X, p.Asp926Glu	p.Ile897Asn, p.Arg1005Cys
Gender	M	F	F	M
Current age (years)	27	30	16	17
Intellectual disability	mild	mild	moderate	mild
Cognitive regression	–	–	–	–
Seizures	–	–	–	–
Initial motor development	normal	normal	normal	normal
Age of onset (years)	3	3	2	4
Motor deterioration	–	–	–	+
Wheelchair use	–	–	–	+
Optic atrophy	–	–	–	–
Myopia	+	+	–	+
Nystagmus	+	+	–	–
Abnormal pursuit	+	+	+	–
Vertical gaze limitation	+	+	+	–
Dysphagia	–	–	+	–
Hypersalivation	–	–	–	–
Cerebellar signs	+	+	+	+
Tremor	–	+	+	+
Babinski refex	–	–	–	–
Spasticity	–	–	mild	–
Peripheral nerve involvement	–	–	–	–
Nerve biopsy	NA	NA	NA	NA
Hypodontia	–	–	–	–
Hypogonadism	+	+	–	–

NA is an abbreviation for not available.

detected with NextGENe. Called SNVs were annotated with SeattleSeq Annotation.

We adopted a prioritization scheme to identify the pathogenic mutation in each individual, similar to the approach taken by recent studies (Table S2).[8–10] First, we excluded the variants registered in the dbSNP131 or 1000 Genome Project from all the detected variants. Then, SNVs commonly detected by MAQ and NextGENe analyses were selected as highly confident variants; 364 to 374 SNVs of nonsynonymous (NS) or canonical splice-site (SP) changes, along with 113 to 124 small insertions or deletions (indels), were identified per individual. We also excluded variants found in our 55 in-house exomes, which are derived from 12 healthy individuals and 43 individuals with unrelated diseases, reducing the number of candidate variants to ~250 per individual. Assuming that HCAHC is an autosomal-recessive disorder based on two affected individuals in one pedigree (individuals 1 and 2), we focused on rare heterozygous variants that are not registered in the dbSNP or in our in-house 55 exomes.

We surveyed all genes in each individual for two or more NS, SP, or indel variants. We found three to eight candidate genes per individual (Table S2). Among them, only *POLR3B* encoding RPC2, the second largest subunit of RNA Polymerase III (Pol III), was common in two individuals (individuals 1 and 3). The inheritance of the variants in *POLR3B* (transcript variant 1, NM_018082.5) was examined by Sanger sequencing. In individual 1, we confirmed that a canonical splice-site mutation (c.1857-2A>C [p.Asn620_Lys652del]), 2 bp upstream of exon 18, was

inherited from his father, and that a missense mutation (c.2303G>A [p.Arg768His]) in exon 21 were inherited from his mother (Figure 1A). The two mutations were also present in an affected elder sister (individual 2) but not present in a healthy elder brother. In individual 3, we confirmed that a nonsense mutation (c.1648C>T [p.Arg550X]) in exon 16 was inherited from her father and that a missense mutation (c.2778C>G [p.Asp926Glu]) in exon 24 was inherited from her mother (Figure 1A). The two mutations were not present in a healthy younger brother. To examine the mutational effects of c.1857-2A>C and c.1648C>T, reverse transcription PCR and sequencing with total RNA extracted from lymphoblastoid cells derived from the individuals was performed as previously described.[11] We demonstrated that the c.1857-2A>C mutation caused deletion of exon 18 from the *POLR3B* mRNA (Figures 2A–2C), resulting in an in-frame 33 amino acid deletion (p.Asn620_Lys652del) from RPC2 (Figure 1B). In addition, the mutated transcript harboring the nonsense mutation (c.1648C>T) was found to be expressed at a much lower level compared with the wild-type transcript (Figure 2D). The expression level of the mutated transcript was increased after treatment with 30 μM cycloheximide (CHX),[11] which inhibits nonsense-mediated mRNA decay (NMD), indicating that the mutant transcript underwent NMD (Figure 2D). The two missense mutations (p.Arg768His and p.Asp926Glu) found in the three individuals occurred at evolutionary conserved amino acids (Figure 1B). Among the other candidate genes in individuals 1 and 3, *MSLN* (MIM 601051), encoding mesothelin isoform 1 preproprotein that is cleaved into megakaryocyte potentiating factor and mesothelin, is a potential candidate in the family of individual 1 as its homozygous variant segregated with the phenotype; however, it is expressed in epithelial mesotheliomas, and the mutation affects less conserved amino acid (Table S3). The other candidate genes' variants did not cosegregate with the phenotype. Thus, mutations in *POLR3B* are most likely to cause HCAHC in two families.

In individual 4, in whom no *POLR3B* mutations were found, there were six candidate genes for an autosomal-recessive model. Among them, *POLR3A* (MIM 614258, GenBank accession number NM_007055.3), harboring two missense mutations, appeared to be a primary candidate because it encodes the largest subunit of Pol III (RPC1) (Figure 1A and Table S2). By Sanger sequencing, we confirmed that a missense mutation (c.2690T>A [p.Ile897Asn]) in exon 20 was inherited from his father and that another missense mutation (c.3013C>T [p.Arg1005Cys]) in exon 23 was inherited from his mother (Figure 1A). The two mutations were not present in a healthy younger sister. The two missense mutations (p.Ile897Asn and p.Arg1005Cys) occurred at relatively conserved amino acids (Figure 1B). In total, we found four mutations in *POLR3B* and two mutations in *POLR3A*. Evaluation of the missense mutations by PolyPhen-2 program showed that three mutations (p.Arg768His,

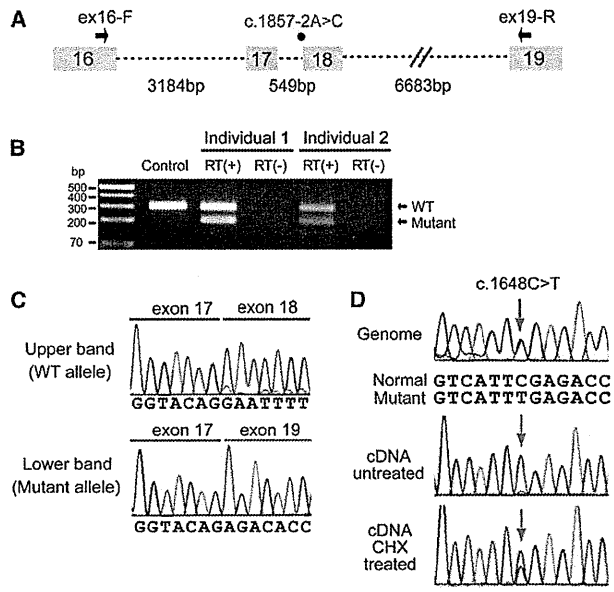

Figure 2. Effects of Splice-Site and Nonsense Mutations in *POLR3B*

(A) Schematic representation of the genomic structure of *POLR3B* from exon 16 to 19. Exons, introns, and primers are shown by boxes, dashed lines, and arrows, respectively. The mutation in intron 17 is depicted as a red dot.

(B) RT-PCR analysis of individuals 1 and 2 with c.1857-2A>C and a normal control. Two PCR products were detected from the individual's cDNA: the upper band is the wild-type (WT) transcript, and the lower band is the mutant. Only a single wild-type amplicon was detected in the control.

(C) Sequence of WT and mutant amplicons clearly showed exon 18 skipping in the mutant allele.

(D) Analysis of the c.1648C>T mutation. Sequence of PCR products amplified with genomic (upper), cDNA from untreated cells (middle), and cDNA from CHX treated cells (lower) as a template. Although untreated cells show extremely low levels of c.1648C>T mutant allele expression, cells treated to inhibit NMD show significantly increased levels of mutant allele expression.

p.Asp926Glu, and p.Ile897Asn) were probably damaging and that p.Arg1005Cys is tolerable. The c.2303G>A mutation (*POLR3B*) was found in one allele out of 540 Japanese control chromosomes. The remaining five mutations were not detected in 540 Japanese control chromosomes, indicating that the mutations are very rare in the Japanese population. Among the other candidate genes in individuals 4, *IGSF10*, a member of immunoglobulin superfamily, is a potential candidate because its variants segregated with the phenotype (Table S3); however, considering a close relationship between *POLR3A* and *POLR3B*, and the fact that *POLR3A* mutations have been recently reported in hypomyelinating leukodystrophy (see below),[12] *POLR3A* abnormality is the most plausible culprit for HCAHC in individual 4.

The structure of Pol III[13,14] and Pol II[15,16] is highly homologous, especially in the largest subunits. Thus, we extrapolated the mutations of RPC1 or RPC2 onto the structure of yeast Pol II (Protein Data Bank [PDB] accession number 3GTP)[17] (Figure 1C). RPB1 and RPB2 subunits of

yeast Pol II are homologous to RPC1 and RPC2 of Pol III, respectively. Asn620_Lys652 in RPC2 corresponds to Tyr679_Lys712 in RPB2. The deletion of Asn620_Lys652 (Tyr679_Lys712) would destroy a structural core of RPB2, leading to loss of RPB2 function. In addition, Arg768 (Arg852 in RPB2) interacts with the main-chain carbonyl group of Arg70 of the RPB12 subunit, and Asp926 (Asp1009 in RPB2) interacts with the side chain of Arg48 of the RPB10 subunit of Pol II (Figure 1D). Arg768His (Arg852His) and Asp926Glu (Asp1009Glu) substitutions are considered to disturb these subunit interactions, leading to dysfunction of the polymerase. Therefore, structural prediction suggests that the mutations in *POLR3B* (RPC2) could affect Pol III function. On the other hand, Ile897 and Arg1005 in RPC1 correspond to Val863 and Arg1036 in RPB1, respectively. Ile897 (Val863) has hydrophobic interactions with Leu170 and Pro176 of the RPB5 subunit and with Phe900 (Phe866) of the RPB1 subunit of Pol II (Figure 1E). Ile897Asn (Val863Asn) substitution is likely to disturb this interaction. Arg1005 (Arg1036) stabilizes interaction between RPB1 and RPB8 subunits (Figure 1F). The Arg1005Cys (Arg1036Cys) substitution appears to make this interaction unstable. Thus mutations in *POLR3A* are also predicted to affect Pol III function.

Clinical features of individuals with *POLR3A* or *POLR3B* mutations are presented in Table 1. MRI revealed high-intensity areas in the white matter in T2-weighted images, cerebellar atrophy, and a hypoplastic corpus callosum in all four individuals (Figure 3). Individuals 1 and 2 showed an extremely similar clinical course. They developed normally during their early infancy, i.e., walking unaided at 15 and 14 months, and uttering a few words at 12 and 13 months, respectively. After the age of 3, individual 1 presented with unstable walking and frequent stumbling and falling down, and individual 2 became poor at exercise. They both had severe myopia (corrected visual acuity of 0.7 and 0.5 at most, respectively). They graduated from elementary, junior high, and high schools with poor records, and the intelligence quotient (IQ) of individual 2 was 52 (WAIS-III). In individual 1, unstable walking was prominent at around 18 years, and he could not ride a bicycle because of ataxia; however, he could drive an automobile. Amenorrhea was noted in individual 2, and was successfully treated by hormone therapy. Individual 1 showed several signs of hypogonadism, including absence of underarm and mustache hair, thin pubic hair (Tanner II), and serum levels of testosterone, follicle stimulating hormone, and luteinizing hormone that were below normal for age 27. Neurological examination of both individuals revealed mild horizontal nystagmus, slowing of smooth-pursuit eye movement, and gaze limitation, especially in vertical gazing, hypotonia, mildly exaggerated deep-tendon reflex (patellar and Achilles tendon reflex) with negative Babinski reflex, and cerebellar signs and symptoms, including ataxic speech, wide-based ataxic gait, dysdiadochokinesis, and dysmetria. Clinical information for individual 3 has been reported previously.[6] Additional findings are as follows: slowing of smooth-pursuit eye movement, gaze limitation in vertical gazing, normal auditory brain responses (ABR), cerebral symptoms with mild spasticity, and intellectual disability (an IQ of 43 according to the WISC-III test), and no myopia but hypermetropic astigmatism. She showed no deterioration besides a mild dysphagia and walks herself to a school for the disabled. Individual 4 developed normally during his

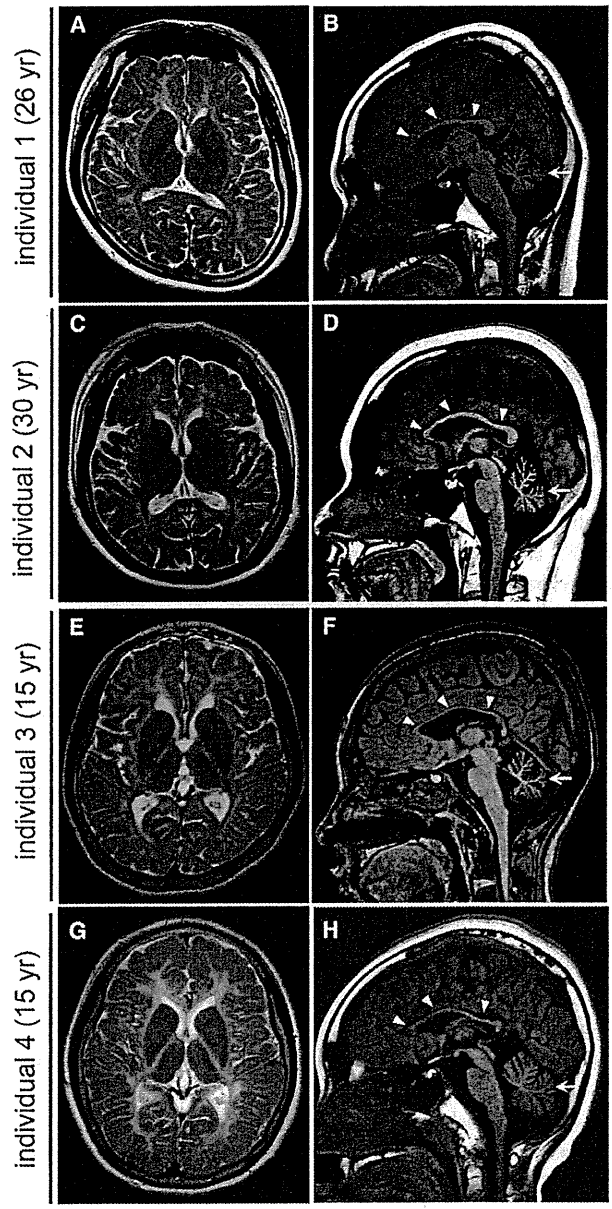

Figure 3. Brain MRI of Individuals with *POLR3B* and *POLR3A* Mutations

(A, C, E, and G) T2-weighted axial images through the basal ganglia. High-intensity areas in the white matter were observed in all individuals.

(B, D, F, and H) T1-weighted midline sagittal images. All the individuals showed hypoplastic corpus callosum (arrowheads) and atrophy of cerebellum (arrows).

early infancy, had normal head control at 3 months, was speaking a few words at 12 months, and was walking unaided at 14 months. His parents noted mild tremors around 4 years. He had normal stature, weight, and head circumference. Although he had severe myopia, his eye movement was smooth with no limitation or nystagmus. He had sensory neuronal deafness on the left side. He showed normal muscle tone and had no spasticity or rigidity. His tendon reflexes were slightly elevated with a negative Babinski reflex. Cerebellar signs were noted; expressive ataxic explosive speech, intension tremor, poor finger to nose test, dysdiadochokinesis, dysmetria, and wide-based ataxic gait. His intelligence quotient was 57 (according to the WISC-III test). His peripheral nerve conduction velocity was within the normal range and his ABR showed normal responses on the right side. He suffered motor deterioration around age 14 and became wheelchair bound.

In this study, we successfully identified compound heterozygous mutations in *POLR3A* and *POLR3B* in individuals with HCAHC. Very recently, Bernard et al.[12] reported that *POLR3A* mutations cause three overlapping leukodystrophies, including 4H syndrome, suggesting that HCAHC is, at least in part, within a wide clinical spectrum caused by *POLR3A* mutations. The p.Arg1005Cys mutation was shared between individual 9 in their report and our individual 4. All 19 individuals with *POLR3A* mutations showed progressive upper motor neuron dysfunction and cognitive regression. In addition, individual 9 showed abnormal eye movement, hypodontia, and hypogonadism. None of these features were recognized in our individual 4; these differences further support phenotypic variability of *POLR3A* mutations.[12] Given the phenotypic similarities among 4H syndrome, HCAHC, and H-ABC, there is a possibility that H-ABC is also allelic and caused by recessive mutations in either *POLR3A* or *POLR3B*.

Pol III consists of 17 subunits and is involved in the transcription of small noncoding RNAs, such as 5S ribosomal RNA (rRNA), U6 small nuclear RNA (snRNA), 7SL RNA, RNase P, RNase MRP, short interspersed nuclear elements (SINEs), and all transfer RNAs (tRNAs). Pol III-transcribed genes are classified into three types based on promoter elements and transcription factors. 5S rRNA is a solo type I gene. Type II genes include tRNA, 7SL RNA, and SINEs. Type III genes include U6 snRNA, RNase P, and RNase MRP.[18–20] The Pol III system is important for cell growth in yeast, and its transcription is tightly regulated during the cell cycle.[20] In zebrafish, *polr3b* mutant larvae that have a deletion of 41 conserved amino acids (Δ239-279) from the Rpc2 protein showed a proliferation deficit in multiple tissues, including intestine, endocrine pancreas, liver, retina and terminal branchial arches.[21] In the mutants, the expression levels of tRNA were significantly reduced, whereas the level of 5S rRNA expression was not changed, suggesting that this *polr3b* mutation can differentially affect Pol III target promoters.[21] RPC2 contributes to the catalytic activity of the polymerase and forms the active center of the polymerase together with the largest subunit, RPC1.[22] Thus, it is reasonable to consider that mutations in *POLR3A* and *POLR3B* cause overlapping phenotypes. Indeed, three individuals with *POLR3B* mutations showed diffuse cerebral hypomyelination, atrophy of the cerebellum and corpus callosum, and abnormal eye movements that overlap with *POLR3A* abnormalities.[12] Furthermore, two out of three individuals showed hypogonadism, suggesting a common pathological mechanism between *POLR3A* and *POLR3B* mutations. In the zebrafish *polr3b* mutants there were no defects of the central nervous system other than a reduced size of the retina, probably reflecting species differences; however, the reduced level of tRNA in the *polr3b* mutants raises the possibility that defects of tRNA transcription by Pol III could be a common pathological mechanism underlying *POLR3A* and *POLR3B* mutations. Supporting this idea, mutations in two genes involved in aminoacylation activity of tRNA synthetase cause defects of myelination in central nervous system: *DARS2* (MIM 610956) and *AIMP* (MIM 603605).[23,24] In addition, mutations in four genes encoding aminoacyl-tRNA synthetase cause Charcot-Marie-Tooth disease (MIM 613641, 613287, 601472, and 608323), resulting from demyelination of peripheral nerve axons: *KARS* (MIM 601421), *GARS* (MIM 600287), *YARS* (MIM 603623), and *AARS* (MIM 601065).[25–28] Thus, it is very likely that regulation of tRNA expression is essential for development and maintenance of myelination in both central and peripheral nervous systems.

An interesting clinical feature of *POLR3B* mutations is the absence of motor deterioration. All three individuals with *POLR3B* mutations could walk without support at ages 16, 27, and 30, whereas individual 3 with *POLR3A* mutations had motor deterioration around age 14. Bernard et al.[12] also reported progressive upper motor neuron dysfunction and cognitive regression in individuals with *POLR3A* mutations. Thus, there is a possibility that phenotypes caused by *POLR3A* mutations could be more severe and progressive than *POLR3B* mutant phenotypes. Identification of a greater number of cases with *POLR3B* mutations is required to confirm this hypothesis.

In conclusion, our data, together with that of a previous report,[12] demonstrate that mutations in Pol III subunits cause overlapping autosomal-recessive hypomyelinating disorders. Establishment of an animal model will facilitate our understanding of the pathophysiology of the multiple defects caused by Pol III mutations.

Supplemental Data

Supplemental Data include three tables and can be found with this article online at http://www.cell.com/AJHG/.

Acknowledgments

We would like to thank all the individuals and their families for their participation in this study. This work was supported by

research grants from the Ministry of Health, Labour, and Welfare (H.S., H.O., M.S., J.T., N. Miyake, K.I. and N. Matsumoto), the Japan Science and Technology Agency (N. Matsumoto), a Grant-in-Aid for Scientific Research on Innovative Areas (Foundation of Synapse and Neurocircuit Pathology) from the Ministry of Education, Culture, Sports, Science and Technology of Japan (N. Matsumoto), a Grant-in-Aid for Scientific Research from Japan Society for the Promotion of Science (H.O., N. Matsumoto), a Grant-in-Aid for Young Scientist from Japan Society for the Promotion of Science (H.S.). This work has been done at Advanced Medical Research Center, Yokohama City University.

Received: August 31, 2011
Revised: October 5, 2011
Accepted: October 10, 2011
Published online: October 27, 2011

Web Resources

The URLs for data presented herein are as follows:

ClustalW, http://www.genome.jp/tools/clustalw/
dbSNP, http://www.ncbi.nlm.nih.gov/projects/SNP/
Ensembl, http://uswest.ensembl.org/index.html
GenBank, http://www.ncbi.nlm.nih.gov/Genbank/
Online Mendelian Inheritance in Man, http://www.omim.org
PolyPhen-2, http://genetics.bwh.harvard.edu/pph2/
Protein Data Bank, http://www.pdb.org/pdb/home/home.do
PyMOL, http://www.pymol.org/
SeattleSeq Annotation, http://gvs.gs.washington.edu/SeattleSeq Annotation/

References

1. Schiffmann, R., and van der Knaap, M.S. (2009). Invited article: an MRI-based approach to the diagnosis of white matter disorders. Neurology *72*, 750–759.
2. Timmons, M., Tsokos, M., Asab, M.A., Seminara, S.B., Zirzow, G.C., Kaneski, C.R., Heiss, J.D., van der Knaap, M.S., Vanier, M.T., Schiffmann, R., and Wong, K. (2006). Peripheral and central hypomyelination with hypogonadotropic hypogonadism and hypodontia. Neurology *67*, 2066–2069.
3. Wolf, N.I., Harting, I., Boltshauser, E., Wiegand, G., Koch, M.J., Schmitt-Mechelke, T., Martin, E., Zschocke, J., Uhlenberg, B., Hoffmann, G.F., et al. (2005). Leukoencephalopathy with ataxia, hypodontia, and hypomyelination. Neurology *64*, 1461–1464.
4. Wolf, N.I., Harting, I., Innes, A.M., Patzer, S., Zeitler, P., Schneider, A., Wolff, A., Baier, K., Zschocke, J., Ebinger, F., et al. (2007). Ataxia, delayed dentition and hypomyelination: a novel leukoencephalopathy. Neuropediatrics *38*, 64–70.
5. van der Knaap, M.S., Naidu, S., Pouwels, P.J., Bonavita, S., van Coster, R., Lagae, L., Sperner, J., Surtees, R., Schiffmann, R., and Valk, J. (2002). New syndrome characterized by hypomyelination with atrophy of the basal ganglia and cerebellum. AJNR Am. J. Neuroradiol. *23*, 1466–1474.
6. Sasaki, M., Takanashi, J., Tada, H., Sakuma, H., Furushima, W., and Sato, N. (2009). Diffuse cerebral hypomyelination with cerebellar atrophy and hypoplasia of the corpus callosum. Brain Dev. *31*, 582–587.
7. Li, H., Ruan, J., and Durbin, R. (2008). Mapping short DNA sequencing reads and calling variants using mapping quality scores. Genome Res. *18*, 1851–1858.
8. Doi, H., Yoshida, K., Yasuda, T., Fukuda, M., Fukuda, Y., Morita, H., Ikeda, S., Kato, R., Tsurusaki, Y., Miyake, N., et al. (2011). Exome sequencing reveals a homozygous *SYT14* mutation in adult-onset, autosomal-recessive spinocerebellar ataxia with psychomotor retardation. Am. J. Hum. Genet. *89*, 320–327.
9. Pierce, S.B., Walsh, T., Chisholm, K.M., Lee, M.K., Thornton, A.M., Fiumara, A., Opitz, J.M., Levy-Lahad, E., Klevit, R.E., and King, M.C. (2010). Mutations in the DBP-deficiency protein HSD17B4 cause ovarian dysgenesis, hearing loss, and ataxia of Perrault Syndrome. Am. J. Hum. Genet. *87*, 282–288.
10. Gilissen, C., Arts, H.H., Hoischen, A., Spruijt, L., Mans, D.A., Arts, P., van Lier, B., Steehouwer, M., van Reeuwijk, J., Kant, S.G., et al. (2010). Exome sequencing identifies *WDR35* variants involved in Sensenbrenner syndrome. Am. J. Hum. Genet. *87*, 418–423.
11. Saitsu, H., Kato, M., Okada, I., Orii, K.E., Higuchi, T., Hoshino, H., Kubota, M., Arai, H., Tagawa, T., Kimura, S., et al. (2010). *STXBP1* mutations in early infantile epileptic encephalopathy with suppression-burst pattern. Epilepsia *51*, 2397–2405.
12. Bernard, G., Chouery, E., Putorti, M.L., Tetreault, M., Takanohashi, A., Carosso, G., Clement, I., Boespflug-Tanguy, O., Rodriguez, D., Delague, V., et al. (2011). Mutations of *POLR3A* Encoding a Catalytic Subunit of RNA Polymerase Pol III Cause a Recessive Hypomyelinating Leukodystrophy. Am. J. Hum. Genet. *89*, 415–423.
13. Jasiak, A.J., Armache, K.J., Martens, B., Jansen, R.P., and Cramer, P. (2006). Structural biology of RNA polymerase III: subcomplex C17/25 X-ray structure and 11 subunit enzyme model. Mol. Cell *23*, 71–81.
14. Fernández-Tornero, C., Böttcher, B., Riva, M., Carles, C., Steuerwald, U., Ruigrok, R.W., Sentenac, A., Müller, C.W., and Schoehn, G. (2007). Insights into transcription initiation and termination from the electron microscopy structure of yeast RNA polymerase III. Mol. Cell *25*, 813–823.
15. Cramer, P., Bushnell, D.A., and Kornberg, R.D. (2001). Structural basis of transcription: RNA polymerase II at 2.8 angstrom resolution. Science *292*, 1863–1876.
16. Gnatt, A.L., Cramer, P., Fu, J., Bushnell, D.A., and Kornberg, R.D. (2001). Structural basis of transcription: an RNA polymerase II elongation complex at 3.3 A resolution. Science *292*, 1876–1882.
17. Wang, D., Bushnell, D.A., Huang, X., Westover, K.D., Levitt, M., and Kornberg, R.D. (2009). Structural basis of transcription: backtracked RNA polymerase II at 3.4 angstrom resolution. Science *324*, 1203–1206.
18. Oler, A.J., Alla, R.K., Roberts, D.N., Wong, A., Hollenhorst, P.C., Chandler, K.J., Cassiday, P.A., Nelson, C.A., Hagedorn, C.H., Graves, B.J., and Cairns, B.R. (2010). Human RNA polymerase III transcriptomes and relationships to Pol II promoter chromatin and enhancer-binding factors. Nat. Struct. Mol. Biol. *17*, 620–628.
19. Dieci, G., Fiorino, G., Castelnuovo, M., Teichmann, M., and Pagano, A. (2007). The expanding RNA polymerase III transcriptome. Trends Genet. *23*, 614–622.
20. Dumay-Odelot, H., Durrieu-Gaillard, S., Da Silva, D., Roeder, R.G., and Teichmann, M. (2010). Cell growth- and differentiation-dependent regulation of RNA polymerase III transcription. Cell Cycle *9*, 3687–3699.

21. Yee, N.S., Gong, W., Huang, Y., Lorent, K., Dolan, A.C., Maraia, R.J., and Pack, M. (2007). Mutation of RNA Pol III subunit *rpc2/polr3b* Leads to Deficiency of Subunit Rpc11 and disrupts zebrafish digestive development. PLoS Biol. *5*, e312.
22. Werner, M., Thuriaux, P., and Soutourina, J. (2009). Structure-function analysis of RNA polymerases I and III. Curr. Opin. Struct. Biol. *19*, 740–745.
23. Scheper, G.C., van der Klok, T., van Andel, R.J., van Berkel, C.G., Sissler, M., Smet, J., Muravina, T.I., Serkov, S.V., Uziel, G., Bugiani, M., et al. (2007). Mitochondrial aspartyl-tRNA synthetase deficiency causes leukoencephalopathy with brain stem and spinal cord involvement and lactate elevation. Nat. Genet. *39*, 534–539.
24. Feinstein, M., Markus, B., Noyman, I., Shalev, H., Flusser, H., Shelef, I., Liani-Leibson, K., Shorer, Z., Cohen, I., Khateeb, S., et al. (2010). Pelizaeus-Merzbacher-like disease caused by AIMP1/p43 homozygous mutation. Am. J. Hum. Genet. *87*, 820–828.
25. Latour, P., Thauvin-Robinet, C., Baudelet-Méry, C., Soichot, P., Cusin, V., Faivre, L., Locatelli, M.C., Mayençon, M., Sarcey, A., Broussolle, E., et al. (2010). A major determinant for binding and aminoacylation of tRNA(Ala) in cytoplasmic Alanyl-tRNA synthetase is mutated in dominant axonal Charcot-Marie-Tooth disease. Am. J. Hum. Genet. *86*, 77–82.
26. McLaughlin, H.M., Sakaguchi, R., Liu, C., Igarashi, T., Pehlivan, D., Chu, K., Iyer, R., Cruz, P., Cherukuri, P.F., Hansen, N.F., et al. (2010). Compound heterozygosity for loss-of-function lysyl-tRNA synthetase mutations in a patient with peripheral neuropathy. Am. J. Hum. Genet. *87*, 560–566.
27. Antonellis, A., Ellsworth, R.E., Sambuughin, N., Puls, I., Abel, A., Lee-Lin, S.Q., Jordanova, A., Kremensky, I., Christodoulou, K., Middleton, L.T., et al. (2003). Glycyl tRNA synthetase mutations in Charcot-Marie-Tooth disease type 2D and distal spinal muscular atrophy type V. Am. J. Hum. Genet. *72*, 1293–1299.
28. Jordanova, A., Irobi, J., Thomas, F.P., Van Dijck, P., Meerschaert, K., Dewil, M., Dierick, I., Jacobs, A., De Vriendt, E., Guergueltcheva, V., et al. (2006). Disrupted function and axonal distribution of mutant tyrosyl-tRNA synthetase in dominant intermediate Charcot-Marie-Tooth neuropathy. Nat. Genet. *38*, 197–202.